Continuous composite hollow-core slabs

Jakob Fisker, PhD student, University of Aarhus, Dept. of Engineering, Denmark
Lars German Hagsten, Prof., Engineering College of Aarhus, Denmark

ABSTRACT

Precast, prestressed hollow core slabs (PPHC-slabs) are traditionally designed as simply supported units with or without concrete topping. When topping is applied, the slabs are often designed to act as composite units, without transverse reinforcement crossing the horizontal interface.
In some situations the design of continuous composite PPHC-slab floors could introduce certain benefits due to an improvement of the Serviceability Limit State behaviour and/or material utilization. Furthermore, depending on the thickness of the topping layer, the application of PPHC-slabs as permanent formwork could introduce increased efficiency with respect to on-site time consumption.
However, the interaction between flexure and shear at internal supports introduces cracks of varying inclination, propagating from the tensile-zone in the topping across the interface into the PPHC-slab. Depending on the extent of cracking, these cracks could ultimately lead to a complete debonding of the horizontal interface.
In order to examine the behaviour of internal supports in composite hollow core slabs and the composite action between hollow-core slabs and topping, several test have been performed. These tests included jointed composite PPHC-slabs subjected to symmetrical three point bending and composite PPHC-slabs subjected to point-loads near support. In the paper, the outcome of the experimental investigations is presented.

Keywords: Hollow-core slabs, Continuity, Composite

INTRODUCTION

Hollow-core slabs are widely used in design of floor-structures in a wide range of different types of buildings. Traditionally, hollow-core slabs are designed to carry the prescribed load as simply-supported units, with or without an additional layer of topping concrete. When topping is present, the hollow-core slab and topping is assumed to act as a composite unit, and the transfer of shear is based solely upon the adhesion at the interface between slab and topping. The performance of such members has previously been investigated experimentally with regards to flexure[1,2] and shear[3,4].

In certain conditions, the construction of continuous composite hollow-core slabs could introduce certain benefits without adding significant changes to construction procedures on-site. As shown below on Fig. 1, the provision of additional reinforcement in the region near intermediate supports constitutes the only significant difference. In some situations, this additional reinforcement is often present anyway due to requirements regarding robustness.

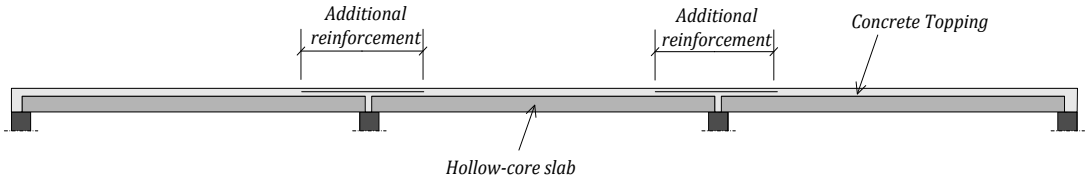

Figure 1: Continuous hollow-core slabs using reinforced concrete topping

The structural enhancements obtained by the provision of continuity are multiple, and would ultimately lead to an improved economic structure. When compared to simply supported hollow-core slabs with topping, the provision of continuity could allow for an improvement of the Serviceability Limit State performance and/or an increase of the ultimate capacity. On the other hand, if the boundary conditions are given beforehand, the presence of intermediate supports capable of transferring bending moments, could lead to a reduction of the volume of the floor-structure, and further reducing the gravity-loads on supporting structures.
Even though used in practice, and considering that design-guidelines have been developed[11,12], the amount of research within this topic is very limited, at least to the knowledge of the authors. Previous tests[5] have been conducted. However, the number of test-specimens was to small in order to extract any definite conclusions. Consequently, many important questions regarding the structural properties and performance of the intermediate joints still remains unanswered.

In order to further investigate some of these properties, a number of tests have been performed at the University of Aarhus. In Fig. 2 below the basic principles of the two test-setups are shown.

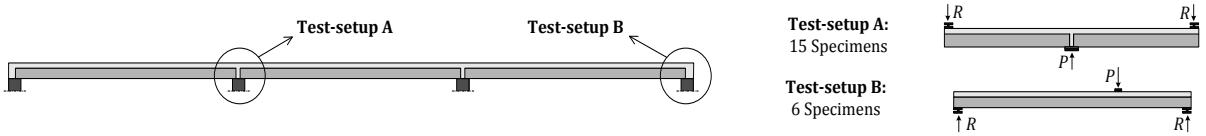

Figure 2: Principles of test-setups

The main subject of the investigations was to evaluate the performance of the region near the intermediate support, when subjected to hogging moments. For this purpose a total of 15 specimens were tested using test-setup A. As can be seen, this setup fulfills the statical conditions near the intermediate supports. However, the geometrical conditions are partially violated.
The provision of continuity leads to a reduction of the reaction at end-supports. However, in order to further investigate the composite action between hollow-core slabs and concrete topping in high shear-stressed regions, a total of 6 specimens were tested using test-setup B.

In the following, the main purposes of the experimental investigations presented in this paper, are briefly introduced.

COMPOSITE BEHAVIOUR
A fundamental precondition for the design of the continuous structure is that the hollow-core slab and the topping concrete is able to act as structural unit. In this context, the unreinforced horizontal interface between hollow-core slab and topping might introduce a certain vulnerability in the case of debonding/delamination. Therefore, it was of interest to observe whether the members failed in a monolithic manner, or if failure was initiated by delamination along the interface. When consulting various codes, the performance of concrete-to-concrete interfaces is normally correlated to surface-roughness - in this case the surface-roughness of the hollow-core slabs. In the tests reported in this paper, the hollow-core slabs were provided with two different surface-textures.

DUCTILITY
Irrespectively of any chosen theory for design (plastic/elastic methods) some degree of ductility of the joints is needed in order to establish a safe and robust structure. If the joints are ductile, a warning of an emergent collapse will be introduced. Furthermore, when considering a restraint structure such as the continuous system considered, regardless of the degree of detail during design, the consequence of time-dependant material parameters, imposed deformations, etc. can only be evaluated approximately. Hence, robustness is needed.
Whether or not, the joints are ductile can be investigated by means of the measured load-displacement-diagrams.

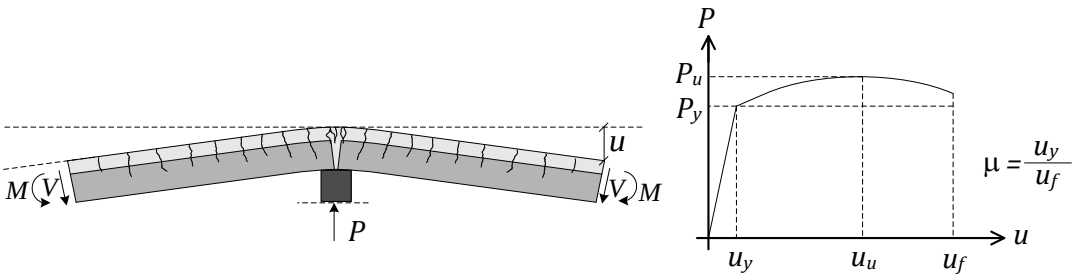

Figure 3: Ductile behaviour of specimens

If the specimens exhibits a ductile behaviour a distinct plastic plateau should be observed, as seen on Fig. 3. The degree of ductility μ can be quantified by the ratio between the displacement at initiation of the plastic plateau u_y, and the displacement at failure u_f. As known, The Theory of Plasticity has shown to be a valuable tool in order to estimate the capacity of RC-members failing in a ductile mode of failure. Hence, if the specimens prove to be ductile it would be natural to apply this approach when calculating the capacity.

DEVELOPMENT OF PLASTIC HINGES

From design of traditional, normal reinforced concrete beams/plates it is well known, that plastic hinges can develop when reinforcement-yielding has initiated in the most stressed sections. The rate of increase of the rotations within this plastic zone is significantly greater than compared to outside this zone. Hence, when the applied load/displacement is increased further, the plastic zone is extended, and the deflected shape of the member approaches that of two rigid members interconnected by a plastic hinge. An important part of the investigation presented in this paper was to examine whether plastic hinges could actually develop.

ROTATION CAPACITY

As known, the load-carrying capacity of hyper-static RC-beam/plate-structures is governed not only by the development of plastic hinges, but also by the rotation capacity of the hinges. If the rotation capacity of the first developed hinges is insufficient, the capacity of the structure is limited to the load-level corresponding to first reinforcement yielding. On the other hand, if the rotation capacity is sufficient, the capacity of the structure as a whole can be addressed using upper and lower bound solutions derived from the Theory of Plasticity. It has to be noticed, that the sufficiency of a plastic hinge to a great extent is governed by the properties of the system at hand (Geometry, Load-configuration etc.).

It is gradually becoming more widely accepted, that the rotation capacity of plastic hinges is due to widening of cracks in the region of reinforcement-yielding. This has been verified experimentally[6] and constitutes the physical background to a number of theoretical models[7,8]. In the case of shear-reinforced members, the capacity of the hinges is governed by either reinforcement rupture or concrete crushing.

However, when dealing with hyper-static slab-structures, shear reinforcement is in general normally not provided, and research[9] indicates, that the rotation capacity in this case may also be limited by the development of a shear-failure after initiation of reinforcement-yielding.

In such members, the transfer of shear by aggregate interlock plays a crucial role[10], but is gradually reduced due to widening of cracks. Hence, the width of cracks could potentially reach a critical level leading to a shear failure before rupture of reinforcement or crushing of concrete.

The phenomenon can be illustrated using the diagrams in Fig. 4, where the top-diagram displays the relation between maximum applied load and shear-slenderness for a simply supported beam, with the presence of "Kani`s valley". When the shear-slenderness *(a/d)* is increased beyond the point of transition, the maximum load is governed by the flexural capacity. However, as illustrated in the bottom-figure, the rotation capacity may still be limited due to a shear failure initiated by the aforementioned mechanisms.

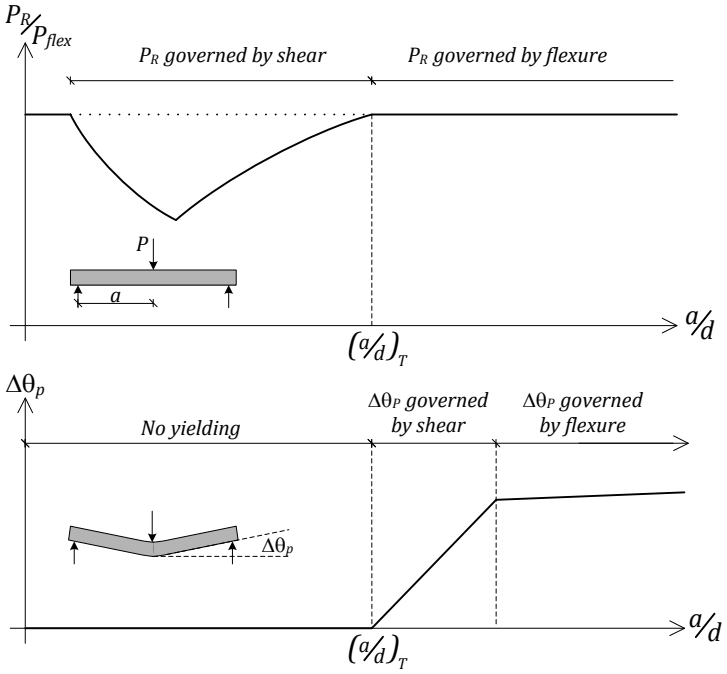

Figure 4: Shear-dependant rotation-capacitiy[9]

For statically determinate members, this is of minor importance. However, in the case of hyper-static structures without shear-reinforcement, the presence of this intermediate zone is of the highest importance in order to estimate the capacity of the structure.

EXPERIMENTAL PROGRAME

TEST SETUP

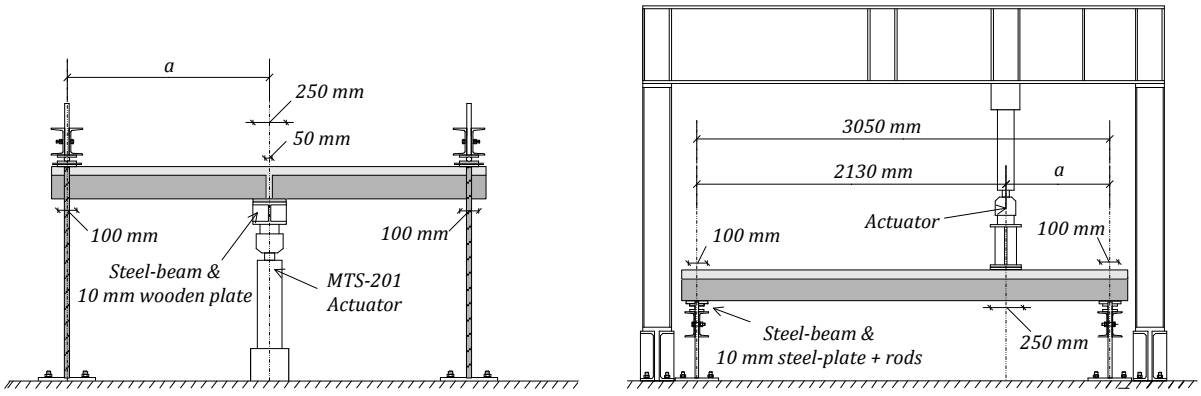

Figure 5: Test-setups; Left: A-series, Right; B-series

The figure above shows the basic principle of the test-setups.

SPECIMENS AND METERIAL-PROPORTIES

A- and B-specimens cross-sections are shown in Fig. 6. The width of the hollow-core slabs was reduced to approx. 70% of the standard-width of 1200 mm, which lead to different shapes of the slab-edges. For the topping a self-compacting concrete was applied.

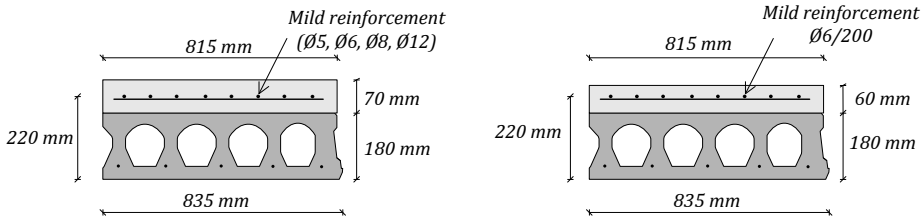

Figure 6: Specimens-sections; Left: A-series, Right: B-series

Table 1 displays different specimen-characteristics for the four different specimen-groups. The bracketed number within the group-names refer to the number of identical specimens within each group. Concrete properties are given as mean-values for each group.

Table 1: Specimen parameters

	a	Reinf.	ρ_L	a/h	W	$f_{c,top}$	$f_{c,hol}$	$f_{ct,top}$	$f_{ct,hol}$
Group	**[mm]**	**[-]**	**[%]**	**[-]**	**[kg]**	**[MPa]**	**[MPa]**	**[MPa]**	**[MPa]**
A1(3)	1425	4Ø6+3Ø8	0,17	5,7	1280	20,2	44,5	nm	nm
A2(3)	1425	4Ø6+7Ø8	0,30	5,7	1280	22,3	48,5	nm	nm
A3(2)	1425	4Ø6+11Ø8	0,42	5,7	1280	20,5	54,4	nm	nm
A4(7)	2195	4Ø5+6Ø12	0,48	8,8	2040	30,1	60,0	nm	nm
B(6)	920	4Ø6	0,07	3,8	1280	22,4	52,8	2,2	2,5

W =Weight of specimens; ρ_L= Longitudinal reinforcement-degree, mild

For the specimens A44-A47 and three of the B-specimens, the surface of the hollow-core slabs was roughened during extrusion using a stiff rake attached to the extruder see Fig. 7. This procedure left the slab-surfaces with a clearly visible macro-roughness of 1-3mm.

Figure 7: Roughening of hollow-core slab surface

The surfaces of the remaining hollow-core slabs were left with standard machine-cast finish. Prior to the application of topping, the surface of the hollow-core slabs were brushed and pre-wetted. After casting of topping, the specimens were wrapped in plastic and stored for at least 14 days. The concrete maturity and compressive strength was monitored using continuous temperature-measurements and cylinder-test

Mild Reinforcement
Table 2 displays the mean-values of the mild-reinforcement used in the topping concrete

Table 2: Mild-Reinforcement properties

	Type	E_s	f_y	f_t / f_y	ε_u
Dim	**[-]**	**[GPa]**	**[MPa]**	**[MPa]**	**[%]**
Ø5	Cold-formed	219	592	1,06	1,7
Ø6	Cold-formed	197	547	1,20	7,3
Ø8	Hot-rolled	178	583	1,07	7,1
Ø12	Hot-rolled	209	598	1,14	5,7

Strain gauges were mounted on the Ø12-bars used for the A4-specimens. However, the preparation of reinforcement for mounting of strain gauges lead to a significant decrease of the elongation capacity of the Ø12-bars. For some of the bars, the ultimate tensile strain capacity was reduced by approx. 45% - from 9,45 to 5,26.

Prestressing
The precast slabs were reinforced with five prestressed strands Ø12.5 with an initial prestressing of 1180 MPa. The mechanical properties of the presetressed reinforcement were not measured prior to the conduction of the tests. The precast prestressed hollow core slabs were manufactured by Danish company A/S Boligbeton, certified under DS/EN ISO 9001.

TEST PROCEDURE
All specimens were tested using displacement-control, and the load was applied according to three different schemes. All three schemes are defined by a number of pre-loading cycles and a final cycle until failure. Each pre-loading cycle contained loading and unloading.
The A1-A3 specimens were subjected to three pre-loading cycles. For the A1-specimens, the amplitude of the pre-loading cycles equaled the load-step when cracking was first observed.

For the A2 and A3 specimens, the amplitude equaled 60% of the estimated yield-load. The A4 specimens were subjected to one cycle of preloading, with an amplitude of 60% of the estimated yield-load.
The B-specimens were also subjected to three cycles of pre-loading. However, the amplitude was increased to 90 % of the estimated capacity.

TEST RESULTS. B-SERIES

OVERALL PERFORMANCE

In Fig. 8 the relationship between the piston-stroke and the applied load is displayed for five of the six tested specimens. The test-series included a total of six specimens. However, one of the specimens failed in an anchorage-failure, due to the development of a flexural crack underneath the applied load, and has been excluded. BR-specimens refer to the specimens with a roughened surface.

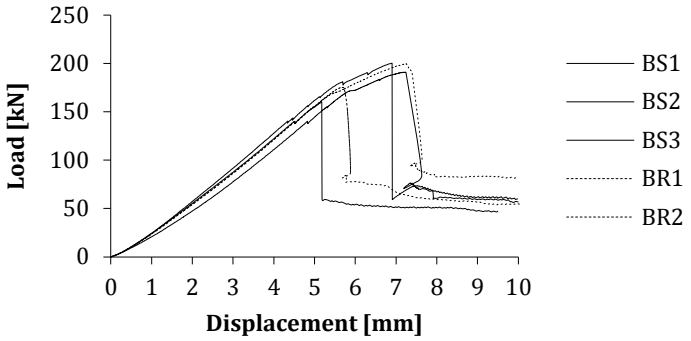

Figure 8: Load-displacement diagrams

As can be seen from the load-deflection diagrams, the specimens exhibited a very rigid and almost perfect linear-elastic response before failure. Just prior to failure a minor degree of softening initiates. However, no cracks were visible on the specimens-surfaces at this load-level.
The failure was significantly brittle, and came suddenly without any indications. Immediately after the propagation of the of line of failure, the applied load dropped, and equilibrium was re-established due to the presence of the prestressed reinforcement.

MODE OF FAILURE

In Fig. 9 below the line of failure related to specimen BR2 is shown. The remaining specimens failed in an identical manner.

Figure 9: Typical mode of failure. Left; BR2, Right; BS2

At failure, a crack/failure-line propagated from the bottom-side near the support towards the point of load-application. In most cases, the line of failure propagated horizontally just underneath the loading-plate. This can be seen on Fig. 9, right, which displays specimen BS2 after a small increase in the applied displacement beyond failure. Hence, the parts on either side of the line of failure was not completely separated during failure.

Based on the observation on the front-side of the specimens, the interface between topping and hollow core slab did not seem to induce any disturbances on the propagation of the crack and the subsequent line of failure. On the backside, however, minor horizontal cracks were observed along the interface. In order to investigate the extent of these cracks, the specimens were cut open after the test, se Fig. 10. The picture shows the section close to the point of load-application, where the line of failure runs within the topping concrete.

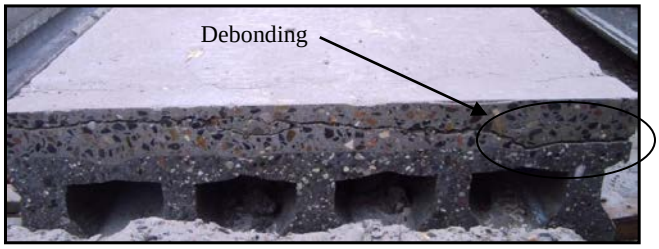

Figure 10: Localized debonding at interface

As can be seen, these disturbances were found to be localized to a zone near the back-side, where the topping and hollow core slabs were completely separated. (Right side on picture). It is not fully understood what may have caused the localized separation between hollow-core slabs and concrete topping. The same phenomena has been observed in other tests[3], where slabs of reduced widths have been used. On the other hand, in experimental investigations[1,2,5] involving slabs of full width, this has not been reported.

SHEAR CAPACITY

Table 3 shows the failure-load and the corresponding shear-capacity relative to the self-weight of the specimens.

Table 3: Maximum load & shear capacity of specimens

	BR1	**BR2**	**BS1**	**BS2**	**BS3**	**Avg.**	**Std.**
	[kN]	**[kN]**	**[kN]**	**[kN]**	**[kN]**	**[kN]**	**[kN]**
P_u	190,9	200,2	160,2	175,2	199,5	-	-
V_u	133,3	139,8	111,9	122,4	139,3	**129,3**	**10,7**

In average, the capacity reached 129,3 kN with a standard deviation of 10.7 kN

TEST RESULTS - A-SERIES

OVERALL PERFOMANCE

Fig. 11 below displays the relationship between the applied load and the midpoint-displacement given as the piston stroke of the actuator. As mentioned earlier, the specimens were pre-loaded before the final cycle. The load-displacements diagrams related to these cycles are not shown. A range of different parameters describing the characteristics of the load-displacement diagrams are given in Table 4 below - all relative to the self weight of the specimens.

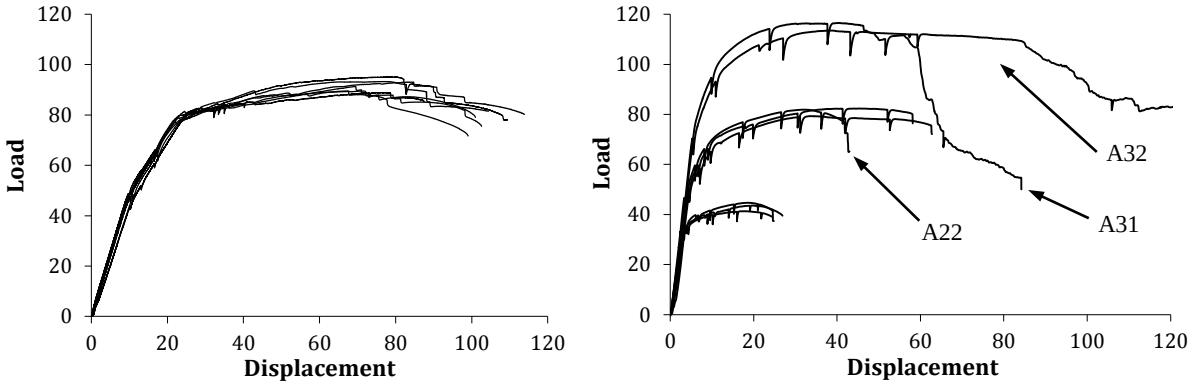

Figure 11: Load vs. Midpoint-displacement. Left; A4, Right; A1-A3

All specimens cracked during the first pre-loading cycle, and the corresponding cracking load P_{cr} is also given in Table 4. All specimens within the groups A1, A2 and A4 failed in a flexural failure due to rupture of the reinforcement. Specimens A31 and A32 failed in a completely different manner, without rupture of any of the reinforcement bars. Furthermore, as can be seen from the load-displacement diagrams, a quite noticeable descending branch was observed for these two specimens. In the case of the A3-specimens u_f represents the initiation of this descending branch.

Table 4: Characteristic parameters obtained from load-disp.-diagrams

	A11	A12	A13	A21	A22	A23	A31	A32	A41	A42	A43	A44	A45	A46	A47
P_{cr}	24,0	26,0	27,5	23,5	36,5	21,5	28,5	24,0	25	16,0	18,0	16,0	18,5	13,5	16,0
P_y	34,5	37,2	36,2	68,5	65,5	70,0	100,0	98,5	80,9	80,0	80,3	77,2	81,4	77,0	78,5
u_y	4,0	4,4	4,4	11,4	7,9	10,6	11,5	13,1	25,9	23,9	26,4	23,2	23,8	23,0	22,8
P_u	41,3	44,7	43,6	79,3	81,9	82,4	116,5	113,5	88,9	95,1	93,1	89,5	93,3	89,5	91,3
u_u	18,0	18,7	19,6	33,5	31,8	45,3	40,2	39,3	74,8	76,6	83,5	67,5	77,0	71,2	69,4
u_f	24,4	24,9	26,9	62,8	41,6	58,2	46,0	85,0	87,5	107,8	113,7	93,1	89,1	100,7	101,0
μ	6,1	5,7	6,1	5,5	5,3	5,5	-	-	3,4	4,5	4,3	4,0	3,7	4,4	4,4
P_u/P_y	1,2	1,2	1,2	1,2	1,3	1,2	1,2	1,2	1,1	1,2	1,2	1,2	1,1	1,2	1,2

P_{cr}= Estimated cracking-load [kN]; P_y= Estimated yield-load [kN]; P_u= Peak-load [kN]; u_y=Disp. at yield-load [mm]; u_u=Disp. at peak-load [mm]; u_f=Disp. at failure [mm]

CRACKING BEHAVIOUR / MODE OF FAILURE

As mentioned, all specimens cracked during the first pre-loading cycle - the corresponding cracking-load can be seen in Table 4. The first visible crack appeared along one of the vertical interfaces at the joint in the middle. In specimens A1 only one crack developed prior to initiation of reinforcement yielding. Between initiation of yielding and load-peak two more cracks developed at a distance of approx. 300 mm from the joint. However, these cracks were only just visible, while the joint-crack reached approx. 15 mm just before failure. In Fig. 12, left, specimen A12 is shown just before failure.

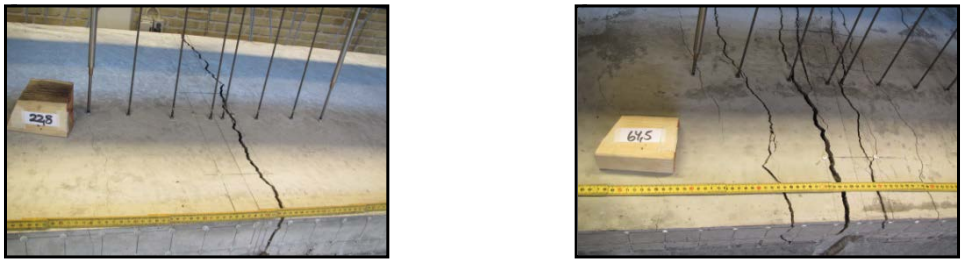

Figure 12: Left; Specimen A12 (u=22,8mm), Right; Specimen A23 (u=64,5mm)

For the remaining specimens multiple cracks were developed before initiation of reinforcement yielding, and the distance between cracks ranged within 100 mm and 250 mm. In specimens A2 and A4 cracks were mostly vertical with none of only a minor inclination. After initiation of reinforcement yielding a minor number of cracks near the joint stated to open extensively and disproportionately to the other cracks, se Fig. 12, right. Ultimately reinforcement was ruptured at the crack in the joint. The specimens failed in a monolithic mode. As in the case of the B-specimens, a zone of localized interface separation was observed near the adjusted edge on the back, se Fig. 10. However, this was not observed in the A4-specimens, where no horizontal cracks were visible.

Fig. 13 displays specimen A31 during failure, after the load-displacement curve had entered the descending branch. Specimen A32 failed in an identical mode, although larger displacements were measured before the complete failure. Before peaking of the applied load, cracks of a certain inclination were clearly visible on either side of the joint, and after the applied load had peaked, one of these cracks suddenly started to open, and became just visible in the compressive zone just above the level of prestressed reinforcement in the hollow core slabs.

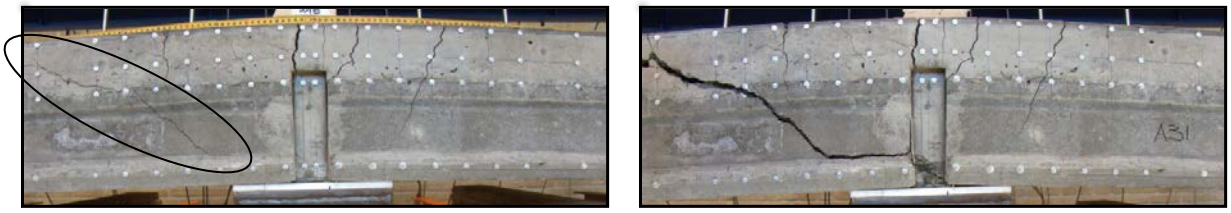

Figure 13: Specimen A31, Left; u=52 mm, Right; u= 65 mm

After a further increase of the applied displacement, the horizontal cracks at the level of the topping reinforcement and near the bottom became clearly visible. Finally, both specimens failed completely in a second failure involving crushing of the concrete in the joint. However, when this occurred the width of the inclined crack/line of failure had exceeded 2-3 mm. Fig. 14 below displays specimen A31 after the test.

Figure 14: Specimen A31 after test

TRANSVERSE DISPLACEMENTS

Transverse displacements were recorded at various positions along the length of the specimens. The diagrams in Fig.15 display the displacements at different load-steps. Only one diagram per specimen-group is shown. The dots indicates the position of the corresponding LVDT, and the thick, red lines represent initiation of yielding, load-peak and failure, respectively. For specimen A31 failure is given as the initiation of the descending branch.

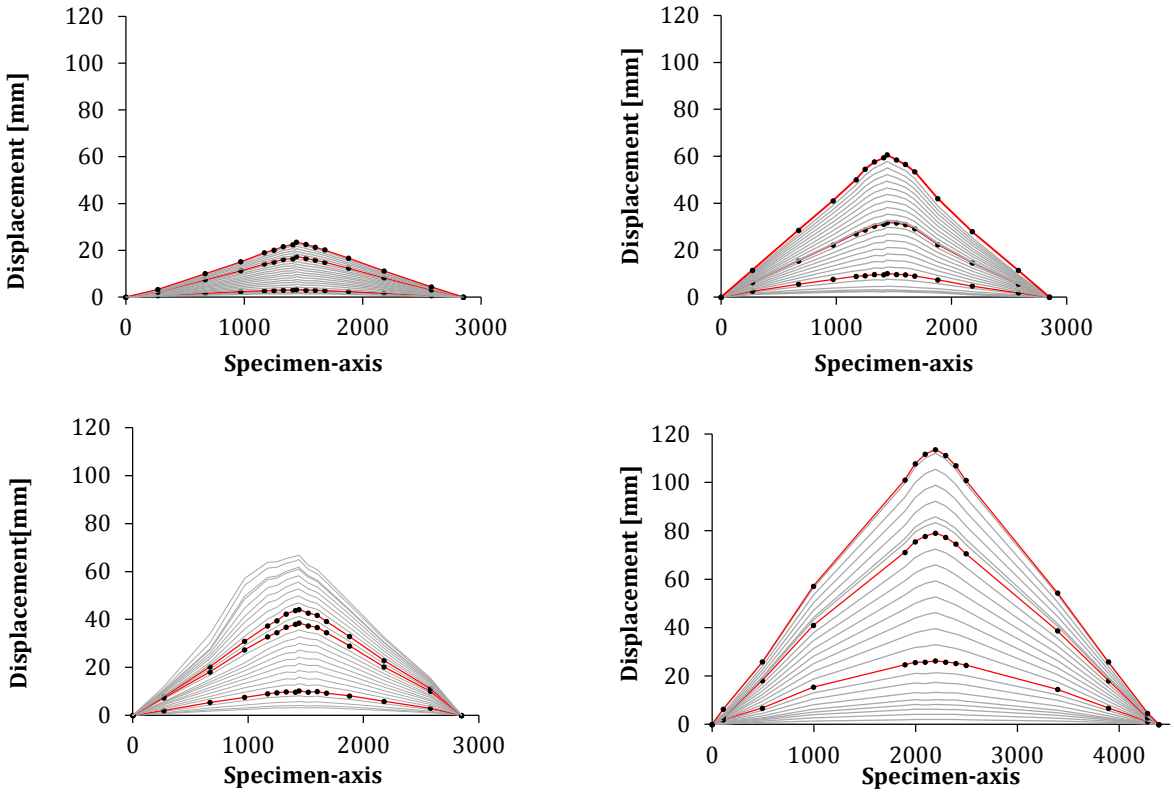

Figure 15: Transverse displacement of A-specimens, Top; A12 & A21, Bottom; A31 & A43

DISCUSSION

A-SPECIMENS

When examining the load-displacement diagrams in Fig. 10 and the corresponding values in Table 4, some important observations can be made. As mentioned, the mode of failure related to the A3-specimens was completely different from the remaining A-specimens. However, these differences did not appear before peak of the applied load.

All specimens exhibited a pronounced and well-defined response before the initiation of reinforcement-yielding, with only very small deviations within each group. For the A1-specimens, the response was approximately linear-elastic with a constant stiffness until initiation of yielding. For the remaining specimens a certain decrease in stiffness is observed when the load reaches approximately 60% of the yield-load. For the A4-specimens the elastic response was almost bi-linear, while non-linearities are clearly visible for the A2- and A3-specimens. It is believed, that these differences are mainly due to the shift from single to multiple cracking combined with increased slenderness of the A4-specimens.

The behaviour of the specimens is also be characterized by a pronounced transition between the elastic range and the post-elastic range, and, within each group, reinforcement-yielding is initiated approximately at the same load-step. Subsequently, all specimens entered a distinct yield-plateau, where the applied load was only slightly increased, while a great increase of the displacements was allowed. As can be seen, the increase of load is approximately of the same order as the ratio between the reinforcement yield-stress and peak-stress (f_t/f_y), emphasizing that a plastic-plateau was in fact developed.

Concerning the A1, A2 and A4 specimens, the failure was indeed ductile. This is also supported by the fact, that all these specimens failed during a flexural failure triggered by rupture of the mild longitudinal reinforcement in the topping concrete. Furthermore, besides the aforementioned localized separation near the one side of the specimens, the specimens appeared to behave monolithic during the complete load-regime. The differences in surface texture of the hollow core slabs did not appear to have any noticeable influence on the behaviour of the specimens.

When comparing the degree of ductility μ between the different groups it appears, that the A1-specimens are the most ductile. In this case, it has to be emphasised that yielding was obtained almost immediately after cracking for the A1-specimens. Hence, the u_y-displacement at first yielding are not directly comparable due to the differences between single cracking and multiple cracking.
Furthermore, very small deformations were recorded for the A1-specimens before yielding, and the influence of errors may therefore be increased relatively.

In Table 6 below, the measured yield- and peak load is compared to the corresponding calculated capacities. The capacities have been calculated using the traditional plastic approach well known from concrete mechanics. As can be seen, only small deviations are obtained.

Table 6: Comparison between calculated and measured capacities

		A11	A12	A13	A21	A22	A23	A41	A42	A43	A44	A45	A46	A47
$P_{y,test}$	[kN]	34.5	37	36.2	68.5	65.5	70	80.9	80	80.3	77.2	81.4	77	78.5
$P_{y,cal}$	[kN]	36.8	36.8	36.8	73	73	73	77	77	77	77	77	77	77
Dev.	[%]	6.2	-1.1	1.6	6.2	10.3	4.1	-5.1	-3.9	-4.3	-0.3	-5.7	0.0	-1.9
$P_{u,test}$	[kN]	41	45	43.6	79.3	81.9	82.4	88.9	95.1	93.1	89.5	93.3	89.5	91.3
$P_{u,cal.}$	[kN]	44.2	44.2	44.2	81	81	81	86.2	86.2	86.2	86.2	86.2	86.2	86.2
Dev.	[%]	7.2	-1.1	1.4	2.1	-1.1	-1.7	-3.1	-10.3	-8.0	-3.8	-8.2	-3.8	-5.9

In Fig. 15 the deflected shape of the A1, A2 and A4-specimens is displayed at different load-steps. The diagrams all reveal that, as the displacements are gradually increased, the change of rotation is gradually becoming localized within the central region around the point of load application. Combined with the fact, that a plastic plateau was actually developed this suggests that plastic hinges are developed.

The corresponding rotation-diagrams are shown in Fig. 16, and have been derived using numerical differentiation. The diagrams evidently supports the supposition, that plastic hinges are developed, and that rigid-body movement is dominating within the post-elastic range.

When considering the A1-specimens, the term "hinge" might be slightly misleading since only a single crack was developed. This is also reflected by the rotation-diagram of A12, where the change of rotation appears to be restricted to a single point.

The deformation-capacity of a plastic hinge is typically defined, as the ability of the hinge to perform angular displacements due to plastic deformations, and is evaluated as the sum of curvatures along the length of the plastic zone.

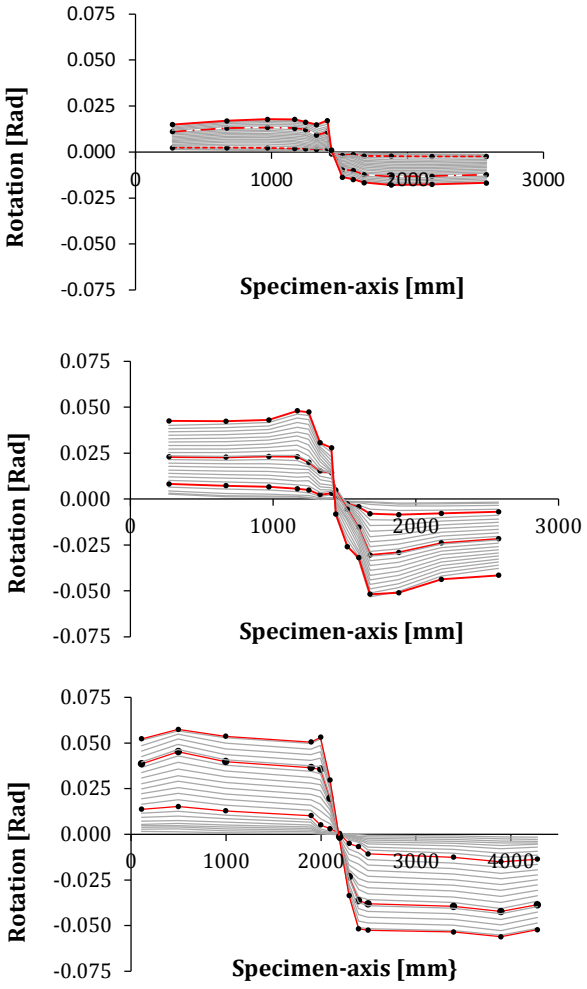

Figure 16: Rotation-diagrams; A12, A21 & A43

Due to the presence of bond-stresses between concrete and reinforcement the plastic zone can be highly discrete, which makes it difficult to address the rotation-capacity of a plastic hinge experimentally.

In this paper, the approximate magnitude of plastic rotations is estimated as the difference between the sum of end-rotations at failure and the sum of the end-rotations at initiation of reinforcement yielding. The end-rotations are estimated using the midpoint-displacement at the corresponding load-level, yielding and failure.

In Table 7, the estimated magnitude of the plastic rotations θ_p are given along with the sum of end-rotations at failure θ_f

Table 7: Estimated rotation capacity

		A11	A12	A13	A21	A22	A23	A41	A42	A43	A44	A45	A46	A47
θ_f	[rad·10^3]	34	35	38	88	58	82	80	98	104	85	81	92	92
θ_p	[rad·10^3]	29	29	32	72	47	67	56	76	80	64	59	71	71

In the graph below in Fig. 17, the estimated plastic rotation is plotted against the corresponding degree of mild reinforcement.

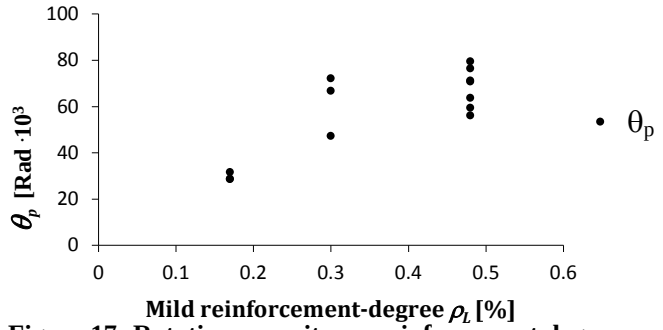

Figure 17: Rotation capacity vs. reinforcement degree

As can be seen, large scatter was obtained, especially among the A4-speciemens, and a more pronounced increase of the capacity was expected. It is not known exactly what caused these results, however, two different factors might have influenced the outcome. First of all, the compressive strength of the topping concrete was higher for the A4-specimens than for the other groups. Hence, the influence of tension-stiffening might have been relatively greater. Secondly, and more importantly, the preparation of reinforcement for mounting of strain gauges lead to a significant decrease of the elongation capacity of the Ø12-bars.

A3-specimens

As stated, the behavior of specimens A31 and A32 was similar to the A2- and A4-specimens when considering the elastic range and the initial part of the plastic plateau. This similarity is also evident from the displacement- and rotation curves, which are shown in Fig. 15 and Fig. 18 for specimen A31, respectively. After yielding, a plastic hinge is developed at midpoint of the specimen, and this behavior continues until the applied displacement reaches the beginning of the descending branch. Subsequently, the gradual development of an additional point of rotation becomes apparent, approximately coinciding with the point of intersection between the topping reinforcement and the crack, that ultimately developed into the line of failure.

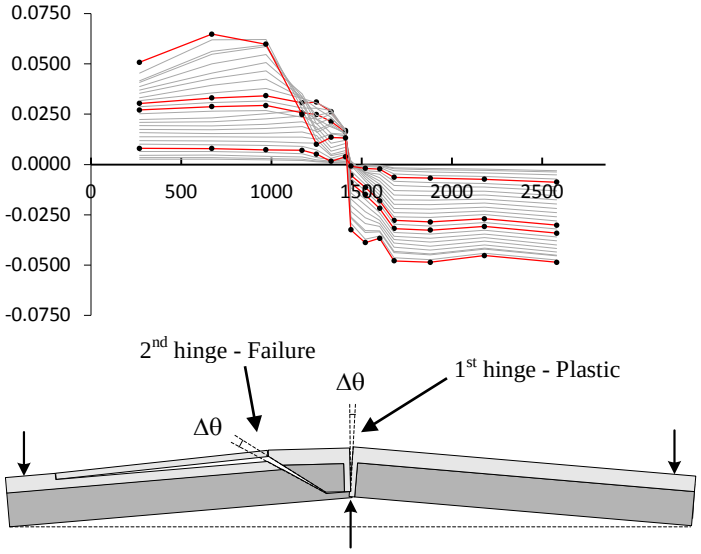

Fig. 18: Rotations, A31

This mode of failure was quite unexpected, and therefore the kinematics of the crack and subsequent line of failure is not known in details. However, it was verified that the line of failure evolved from a flexural crack - clearly visible in the topping concrete.

As can be seen from Fig. 13, the width of the inclined crack/failure line is significant at the onset of concrete crushing (2-3mm), indicating that the magnitude of shear stresses transferred by aggregate interlock along the crack is either zero or greatly reduced. This suggests, that the A3-specimens failed in shear. The shear failure appears to have been initiated due to the fact, that an inclined crack at a critical position reached a critical width, and thereby by exceeding the ultimate shear capacity activated by aggregate interlock. Subsequently, a weakened section has been created, which can also explain the development of an additional "hinge" and the decrease in load, as given by the load-displacement diagrams.

Even though not directly comparable, it can be seen that the apparent shear-capacity of the A3-specimens comprised approximately only 50% of the shear-capacity of the B-specimens, where no cracks were visible before failure. It appears reasonable to speculate that this reduction is due to the shear-flexure cracks introduced by the hogging moment. Furthermore, due to the gradual transfer of prestressing near the end-zone combined with the presence of shear-flexure cracks, the benefits from prestressing might only be marginal.

CONCLUSION

For all of the tested specimens, hollow-core slabs and concrete topping was found to act as a composite unit. For all specimens, localized cracking along the horizontal interface was observed on one side. However, the specimens failed in a monolithic manner, which did not appear to be initiated by this localized interface delamination. This is consistent with other test-results.

In terms of the A-specimens, specifically, a ductile behavior was observed, and with the exception of the A3-specimens, a consistent performance was observed within each specimen-groups. The capacity with regards to yield- and ultimate loads was estimated using a traditional rigid-plastic approach, and sufficient accuracy was obtained.
The investigations also revealed that plastic hinges were able to develop in the zone near the joint.

Regarding the A3-specimens, some degree of discrepancy was observed with respect to the displacement, at which the descending branch was initiated. It is believed, that these specimens failed in a shear due to extensive opening of cracks. However, due to the lack of measurements on the kinematics of the inclined cracks, and the fact that only two specimens were tested, no final conclusions can be made.

These findings suggest, that the simple type of connection tested, to some extent is suitable for design of continuous composite hollow-core slabs. However, the interaction between shear and flexure in the region near the joint must be further investigated in order to gain more knowledge regarding the shear-carrying mechanism when cracks are introduced. Especially, with regards to the influence of shear on the rotation-capacity of the hogging region in composite slabs.

REFERENCES

1. Scott, N.L., “Perfomance of prescast prestressed hollow core slabs with composite concrete topping” *PCI-Journal*, V. 18 1973, pp. 65-77.

2. Ibrahim, I.S., Elliot, K.S., Copeland, S., "Bending Capacity of Precast Prestressed Hollow Core Slabs with Concrete Toppings", *Malaysian Journal of Civil Engineering* 20(2), 2008, pp. 260 - 283.

3. Girhammur, U., Pajari, M., “Tests and analysis on shear strength of composite slabs of hollow core units and concrete topping”, *Construction and Building Materials*, V. 22, 2008, pp. 1708-1722.

4. Ueda, T., Stitmannaithum, B.,“Shear strength of precast prestressed hollow core slabs with concrete topping”, *ACI Structural Journal*, V.88, 1991, pp. 402-410.

5. Tan, K.H., Lian-Xiang, Z., Paramasivam, P., Designing hollow-core slabs for continuity *PCI Journal*, V. 41, 1996, pp. 82-91.

6. Beeby, A.W.,”Ductility in reinforced concrete: Why is it needed and how is it achieved?” *The Structural Engineer*, V. 75,1997, pp. 311-318.

7. Bachmann, H, Influence of Shear and Bond on Rotational Capacity of Reinforced Concrete Beams, *International Association for Bridge and Structural Engineering*, 30(6), 1970, pp. 11-28.

8. Hestbech, L., Fisker, J., Hagsten, L.G., Modeling of Rotational Capacity in RC Linear Elements, *Proceedings of the fib Symposium on Concrete Engineering for Excellence and Efficiency*, Prague, Czech Republic, 8-10 june, 2011.

9. Rodrigues, R.V., Muttoni, A., Fernández Ruiz, M., Influence of Shear on Rotation Capacity of Reinforced Concrete Members Without Shear Reinforcement, *ACI Structural Journ*al, V. 107, No. 5, September-October, 2010

10. Sherwood, E.G., Bentz, B.C., Collins, M.P., Effect of Aggregate Size on Beam-Shear Strength of Thick Slabs, *ACI Structural Journal*, V. 104, No. 2, March-April, 2007

11. Composite Floor Structures, *fib*-Report, 1998

12. Special design considerations for precast prestressed hollow core floors, *fib*-Bulletin No. 6, 2000